Biosensors and Bioelectronics 67 (2015) 553–559

Contents lists available at ScienceDirect

Biosensors and Bioelectronics

journal homepage: www.elsevier.com/locate/bios

Printed and flexible biosensor for antioxidants using interdigitated ink-jetted electrodes and gravure-deposited active layer

Felippe J. Pavinatto [a,b,*], Carlos W. A. Paschoal [c,d,e], Ana C. Arias [a]

[a] EECS – Electrical Engineering and Computer Science, University of California, Berkeley, USA
[b] IFSC – Physics Institute of São Carlos, University of São Paulo, São Carlos, SP, Brazil
[c] DEFIS – Physics Department, Federal University of Maranhão, São Luís, MA, Brazil
[d] Department of Materials Science and Engineering, University of California Berkeley, Berkeley, CA, USA
[e] Department of Physics, University of California Berkeley, Berkeley, CA, USA

ARTICLE INFO

Article history:
Received 7 June 2014
Received in revised form
4 September 2014
Accepted 16 September 2014
Available online 22 September 2014

Keywords:
Biosensor
Antioxidants
Interdigitated-electrodes
Inkjet-printing
Gravure-printing
Plastic electronics

ABSTRACT

Printing techniques have been extensively used in the fabrication of organic electronic devices, such as light-emitting diodes and display backplanes. These techniques, in particular inkjet printing, are being employed for the localized dispensing of solutions containing biological molecules and cells, leading to the fabrication of bio-functional microarrays and biosensors. Here, we report the fabrication of an all-printed and flexible biosensor for antioxidants. Gold (Au) interdigitated electrodes (IDEs) with sub-100 μm features were directly inkjet-printed on plastic substrates using a nanoparticle-based ink. Conductivities as high as 5×10^6 S/m (12% of bulk Au) were attained after sintering was conducted at plastic-compatible 200 °C for 6 h. The enzyme Tyrosinase (Tyr) was used in the active layer of the biosensors, being innovatively deposited by large-area rotogravure printing. A tailor-made ink was studied, and the residual activity of the enzyme was 85% after additives incorporation, and 15.5% after gravure printing. Au IDEs were coated with gravure films of the Tyr-containing ink, and the biosensor was encapsulated with a cellulose acetate dip-coating film to avoid dissolution. The biosensor impedance magnitude increases linearly with the concentration of a model antioxidant, allowing for the construction of a calibration curve. Control experiments demonstrated the molecular recognition characteristic inferred by the enzyme. We found that the biosensor sensitivity and the limit of detection were, respectively, 5.68 Ω/μm and 200 μM. In conclusion, a disposable, light-weight, all-printed and flexible biosensor for antioxidants was successfully fabricated using fast and large-area printing techniques. This opens the door for the fabrication of technological products using roll-to-roll processes.

1. Introduction

Antioxidants are molecules that act as free radical scavengers and help preventing oxidative stress, which causes damage to cells and tissues and is known to be related with some cardiovascular and neurological disorders (Sen and Chakraborty, 2011). Phenol-based antioxidants (specifically poly-phenols) are the most important class of antioxidants in nature, and their mechanism of action is being investigated by scientists worldwide (Fraga et al., 2010). Due to the high content of poly-phenols in products like olive oil and wine, and to the claims that diets like the Mediterranean (rich in those products) help to slow down aging, there is a huge concern nowadays at determining the antioxidant power of foods and beverages.

Biosensors have emerged as a promising tool to quantitatively determine the content of poly-phenols and other kinds of antioxidants in foods and beverages (Prieto-Simón et al., 2008; Mello and Kubota, 2007; Barroso et al., 2011). The naturally occurring enzyme Tyrosinase (Tyr) is the recognition element used in the majority of previous work to infer specificity and selectivity to the devices. The enzyme, also known as poly-phenol oxidase, is able to catalyze two steps of phenols oxidation, to ortho-dihidroxy-phenols and ortho-quinones. There are several ways in which electrodes are modified with Tyr, being physical adsorption or entrapment (frequently in an electropolymerized conducting polymer) the most common ones (Barroso et al., 2011). An alternative and efficient approach is to use nanostructured thin films to chemically anchor and support Tyr layers on conducting electrodes. This has been done by one of the authors of the present paper and led to very efficient biosensors for antioxidants that

* Correspondence to: Av. Trabalhador São Carlense 400, Centro, São Carlos, SP 13566-590, Brazil.
E-mail address: pavinatto@ifsc.usp.br (F.J. Pavinatto).

http://dx.doi.org/10.1016/j.bios.2014.09.039
0956-5663/

reached a detection limit in the order of 10^{-2} μM (Apetrei et al., 2011; Pavinatto et al., 2011). However, despite their good performance and importance for fundamental science, such biosensors have a laborious and intrinsically expensive fabrication process, which greatly reduces their technological potential.

Printing techniques have been employed in the fabrication of large-area thin films over plastic surfaces, giving rise to flexible organic electronics (Arias et al., 2010). Amongst the several types of printing techniques (Kipphan, 2001) are inkjet printing, screen-printing, micro-contact printing, (flexo) gravure and offset methods (Kang et al., 2013; Søndergaard et al., 2013). Biomolecules and biological materials, like proteins, DNA, antibodies, neurons and whole cells (Delaney et al., 2009; Derby, 2008; Ilkhanizadeh et al., 2007; Sanjana and Fuller, 2004; Saunders et al., 2010; Sumerel et al., 2006) have also been deposited onto surfaces by printing methods. The goal is to deposit patterned structures, bio-arrays and even tissue-like materials for bioengineering (Derby, 2012; Villar et al., 2013), and inkjet is the preferred technique in these studies.

Printed biosensors are also well documented in literature (Gonzalez-Macia et al., 2010). For instance, inkjet has been used to fabricate biological arrays for drug-screening (Arrabito et al., 2013), sequentially deposit nano-materials and enzymes (Suman et al., 2011) and to fabricate paper-based micro-fluidic devices (Abe et al., 2008). However, large-area and high throughput printing methods have not been used before for depositing the active layer in bioelectronic devices. Gravure printing presents harsh conditions for biomolecules, such as high shear forces and pressure, and is therefore not largely applied in this type of devices. Reddy et al. (2011a) have described a biological sensor instead of a biosensor, and no biomolecule is gravure printed. Jabrane et al. (2011) used gravure to deposit bacteriophages on paper for bacteria detection using cell cultures, not a bioelectronic device. In another work, the same group describes the printing on paper via gravure of an ink containing the Horseradish Peroxidase (HRP) enzyme (Jabrane et al., 2008). After running a few printing tests, they indirectly measured the oxidation of hydrogen peroxide assisted by the printed film using a colorimetric method, and noticed that high viscosity inks have less catalytic effect. However, the measured activity is not compared to the initial enzyme activity in solution or to a film without enzyme subjected to the same colorimetric test. Therefore, although the potential use of the printed film as a biosensor is claimed in previous reports, no detection measurements or calibration curves are reported.

In this paper we report on the fabrication of a flexible and all-printed biosensor for antioxidants, which uses a combination of inkjet and gravure printing to form high-resolution interdigitated electrodes and deposit the sensor active layer. Special attention is devoted to the fabrication of the device, which involved the optimization of inkjet conditions to deposit electrodes with sub-100 μm features and the development of an enzyme-containing ink for gravure. In addition, the surface energy of flexible substrates was modified to optimize film properties. The detection of a model analyte in a range well below the one polyphenols are found in wines and olive oils is demonstrated, illustrating the potential applicability of the device in biosensing analysis.

2. Materials and methods

Tyrosinase (Tyr) from mushrooms, 5037 Units/mg (T3824), carboxymethyl-cellulose (CMC, 419338), trehalose (T9531) and triton X-100 (X100), were all obtained from Sigma-Aldrich and used as received. Polyethylene terephthalate (PET, R342 3 M), polyethylene naphthalate (PEN, Teonex Q65FA Teijin-DuPont) and a special coated PEN (PQA1, DuPont) were used as plastic substrates for printing. These plastics were, when mentioned, rinsed with isopropyl alcohol (IPA), treated by 10 min ozone exposure (home-made chamber having a Xe lamp and fan system to exhaust gases), or oxygen plasma (TEGAL, Plasmod-50 W) before use. Commercially available nanoparticle-based silver (Ag) ink CCI-300 (Cabot Chemical Co) and gold (Au) ink NPG-J (Harima Chemicals) were used for electrodes inkjet. Cellulose acetate (CA, Aldrich 180955) was used for biosensor encapsulation, and pyrogallol (Pyr, Sigma-Aldrich 254002) as a model analyte in the optical evaluation of enzyme activity and detection measurements.

All the inks, synthesized here or commercially obtained, were filtered with a 0.45 μm Millipore membrane before use in printing tests, and new formulations had their viscosity measured in a DV-III rheometer from Brookfield, and surface tension evaluated with a sensor based on the Wilhelmy method (from KSV NIMA Inc.). The enzymatic activity of Tyr incorporated to the inks was estimated by the change in absorption at 420 nm (generation of purpurogallin (Pur) from Pyr) using a UV–vis spectrophotometer model UV3600 (Shimadzu). Activity (A) was defined by the change in absorption per unit of time per mol of substrate, according to Eq. (1). To determine Tyr activity after printing, the film was re-dissolved with the minimum amount of buffer necessary, which was always less than 1 mL, avoiding large variations in enzyme concentration.

$$A = \frac{\Delta \text{absorbance}}{\Delta t \text{ x mol of substrate}} \times 1000 \quad (1)$$

A Dimatix DMP-2800 inkjet printer (Fujifilm Corp.) with 10 pL (drop volume) cartridges was used for printing metallic electrodes, and conditions for ideal jetting and continuous high resolution patterns formation are discussed below in the text. For rotogravure, a G1-5 printer tester from IGT with a 50 mm wide gravure disk model 402.118 (screen angle of 120°- R60) was used to optimize printing conditions, and a Daetwyler R&D printer (Daetwyler Co) was employed to deposit large area films over the previously prepared interdigitated electrodes once the best speed and force (cylinder pressure) were found. In this case, the custom-made cylinder had a 95×95 mm^2 cell engraved on it.

Surface morphology for the printed films was characterized with an i50 optical microscope (Nikon), a MFP atomic force microscope (AFM) from Asylum and a Dimension 3000 AFM from Veeco (measurements conducted in the tapping mode at 75 kHz using a Multi75Al-G (Budget Sensors) Si tip of 3 N/m tip constant in both cases). The profile of the printed features was analyzed with a DekTak 150 profilometer (Veeco), and resistivity of the metallic electrodes was measured using a 4-point probe apparatus from Signatone (S-302-4) coupled to a HP4145B parameter analyzer (Hewlett-Packard). For the detection measurements, an impedance analyzer HP model 4192A was employed, with the data collected in a customized LabView® (National Instruments) suit. Other relevant experimental details regarding ink preparation, printing, and films characterization are provided in the text along with results.

3. Results and discussion

3.1. Inkjet-printed interdigitated electrodes on plastic

Electrical impedance was elected as detection method in this work because of the simplicity of device fabrication and detection measurements. With this method, additional electrodes, and semiconductor or mediator materials, commonly used in electrochemistry and transistor-based biosensors are dispensed (Varshney and Li, 2009). Interdigitated electrodes (IDEs) allow

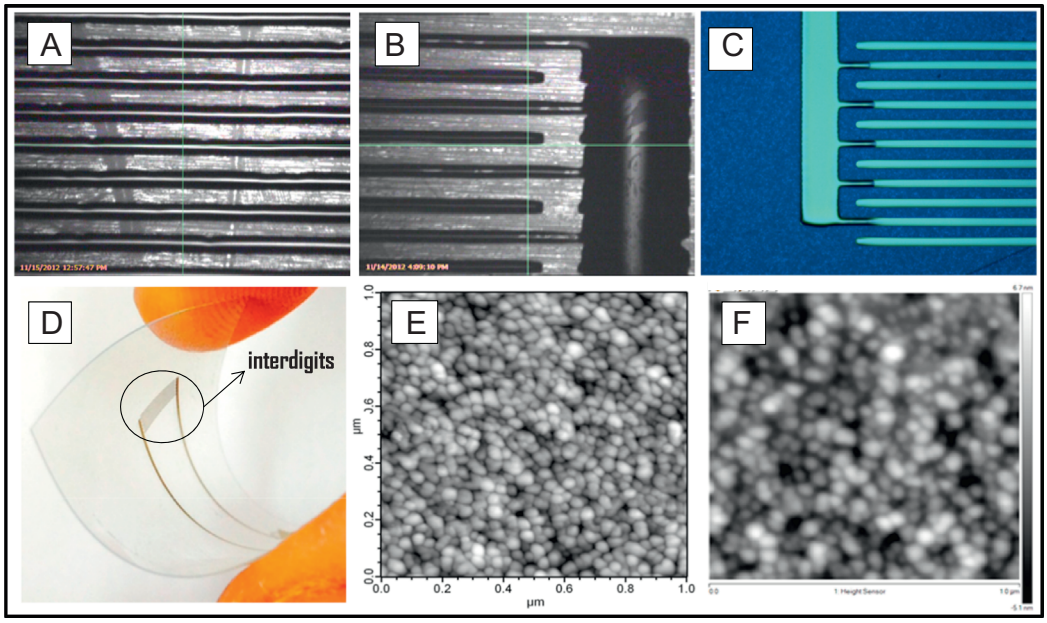

Fig. 1. A) digital picture of Ag IDE ink-jetted on ozone-treated PET; (B) digital picture of Ag IDE ink-jetted on bare PEN; (C) optical microscopy of Au IDE ink-jetted on bare PQA1; (D) photo of the flexible Au IDE inkjet-printed on PQA1; (E) AFM image showing surface morphology for the printed Au electrode after sintering, but before use and bending; (F) AFM image displaying printed Au electrode morphology after use in impedance measurements and after being subjected to 10 flexion cycles in 2 orthogonal axis, parallel and perpendicular to fingers direction.

the amplification of the capacitance signal, and hence of device sensitivity, due to the large active capacitor area and short inter-fingers distance (Berggren et al., 2001). Conventionally, lithographic methods are employed to fabricate IDEs for use in biosensors and biological samples sensing (Tsouti et al., 2011; Varshney and Li, 2009), as features on nanometer scale can be obtained (Singh et al., 2011; Van Gerwen et al., 1998). However, lithography requires labor-intensive procedures, ultraclean environments and expensive machinery, and some of the processes use high temperatures and aggressive chemicals (e.g. etching steps) which are not compatible with plastics.

Inkjet printing has been used for the direct one-step deposition of flexible Ag IDEs (Altenberend et al., 2013; Cho et al., 2007; Claramunt et al., 2013; Correia et al., 2013; Monereo et al., 2013), with features as small as 40 and 30 μm being achieved on PET and Kapton (polyimide), respectively (Correia et al., 2013). Here, Ag IDEs were also inkjet-printed on ozone-treated PET using drop spacing of 30 μm, resulting in 80 μm wide digits (Fig. 1A). Continuous Ag lines and IDEs were printed on PEN, a plastic with improved thermal stability (Fig. 1B), using 20 μm drop-spacing. In this case, no surface treatment or IPA cleaning of the plastic was necessary. Narrower digits and larger spacing were obtained, when comparing to those of PET. Feature sizes for the electrodes are summarized in Table 1.

Although Ag electrodes fabricated by inkjet have high conductivity and can be used in a variety of electronic devices in dry conditions, including biosensors, they very often have poor resistance due to oxidation and degrade when used in aqueous environments under applied electrical potential. This frequently leads to loss of adhesion to the substrate and makes post-printing treatments (as electroplating and coating with a inert dielectric) necessary to stabilize the printed conductors (Altenberend et al., 2013). That was the case for Ag electrodes fabricated in this work, which presented darkening and loss of adhesion when tested in impedance measurements in buffer. For this reason, Au electrodes were pursued since the metal has higher oxidation potential and improved inertness and stability in aqueous environments (e.g. biological fluids).

Table 1
Minimum features found for Ag and Au interdigitated electrodes inkjet-printed on different plastics.

Metal	Substrate	Inter-finger distance (μm)	Finger width (μm)
Ag	PEN	90	60
Ag	PET	65	80
Au	PQA1	75	45

To the best of our knowledge, Au IDEs have not been directly deposited previously by inkjet on plastics in a one-step printing process. There is only one report in literature describing the use of inkjet to pattern a thiol self-assembled monolayer to protect an Au surface from etching in a multi-step process that leaded to interdigits with 100 μm features (Cho et al., 2007). Here, we have used a commercial ink (NPG-J, from Harima Chemicals) to inkjet IDEs on PQA1. In contrast to conventional plastics as PET, PEN and Kapton, where inkjet printing does not render uniform patterned films, PQA1 has a very good match of surface energy for the Au ink surface tension, resulting in optimized spreading and perfectly spherical dots with the diameter of 45 μm. Using 30 μm drop spacing, continuous lines with perfectly smooth edges and 45 μm line-width could be printed. Further tests were conducted in order to find the maximum approach for the lines that can be safely printed with no merging of neighbor fingers, and IDEs were successfully ink-jetted on PQA1. An optical microscopy image and a photo of a flexible 10-pairs Au IDE are shown, respectively, in Fig. 1C and D, and the typical dimensions for the structure is also displayed in Table 1. As can be seen, inkjet have afforded the printing of good quality, homogeneous electrodes with resolutions better than what is usually obtained with gravure or screen-printing (Reddy et al., 2011b; Saum et al., 2000), and with no waste of material.

The recommended sintering conditions for the Au ink is 250 °C for 1 h, but the maximum working temperature for PEN is around 190 °C. In order to solve this conflict, sintering was conducted at lower temperatures and longer times, providing eventually the same amount of thermal energy to the ink. Resistivity was mapped

for several combinations of this two factors (Pavinatto et al., in preparation), and it is seen that the IDEs have resistivity in the order of 10^{-6} Ω m when sintered at 200 °C for 6 hs. Remarkably, the processing of the printed electrodes 10 °C above PQA1 degradation temperatures was enabled by the presence of the inorganic coating on PQA1. Interestingly, a very peculiar dependence of sintering speed on line-width was observed for high resolution features (Pavinatto et al., in preparation), and a systematic fluctuation in line thickness is also present for this fine lines (see Supplementary Fig. S1).

In the AFM image of Fig. 1E it is possible to see that the modified sintering protocol was not sufficient to promote neck formation between particles, which is expected for nanoparticle-based conductors in advanced stages of sintering (Allen et al., 2010). Nevertheless, there was a significant nanoparticle growth from ~12 nm in the ink dispersion (informed by Harima Chemicals) to an average of 50 nm (obtained by measuring tens of particle in the image), which was sufficient to make the film conductive, as mentioned. AFM images were also used to attest the stability of the electrodes to bending and use in impedance measurements. As it can be seen in Fig. 1F, the morphology of the electrodes after use in biosensing and after being subjected to a custom-developed flexibility test (see Supplementary material – flexibility test protocol) is pretty similar to the one they presented right after fabrication, but before use and bending (Fig. 1E). The same morphology, free of cracks, was seen all across the surface of a few digits, and the only difference is that Fig. 1F looks blurred and with particles a little bit bigger than those in E, which is attributed to differences in resolution of the microscopes used to acquire the images (Asylum for E and Veeco for F), and to the accumulation of salt from the buffer used in detection measurements. Finally, the strong adhesion of the electrodes was confirmed by manually pressing down an ordinary lab Kapton tape against them, and then releasing it. No film detachment or visual damage of the printed metal traces was observed even after repeating this simple test several times.

3.2. Tyrosinase-containing ink formulation

As pointed in the introduction section, shear stress in gravure printing is known to be very high, and the only paper that deals with gravure of an enzyme (HRP) does not report comparative studies with the original activity of the enzyme in solution, or the use of the printed film in detection measurements (Jabrane et al., 2008). Here, we aimed at finding a Tyrosinase-based ink formulation that ideally would fulfill both the need for adequate properties for gravure printing and the search for a good environment for the enzyme. A careful selection of additives for the ink was done based on results from papers in literature dealing with the printing of enzyme-containing inks using inkjet (Derby, 2008; Di Risio and Yan, 2007; Kaushik and Bhat, 2003). Two additives firstly incorporated to the pH 7.4 phosphate buffer solvent were triton X-100 and trehalose. Triton is a non-ionic polymeric surfactant, which is much less aggressive to enzymes that charged detergents. The addition of 0.05% v/v of triton X-100 was sufficient to decrease the surface tension of the solvent from 72.0 to 29.4 mN/m, which is adequate for gravure. Trehalose sugar was used as enzyme stabilizer and activity preservative, since the sugar is known to form a stable network of hydrogen bonds and act structuring water molecules, helping proteins to keep their most favorable conformation (Kaushik and Bhat, 2003). A small amount of trehalose was added to the ink (1%) since the concentration of Tyr was also very low (68.5 μg/mL), as in our previous works (Pavinatto et al., 2011).

Carboxymethyl-cellulose (CMC) was selected as viscosity enhancer by being a natural-derived polymer with great power of changing solution viscosity with small increments in its concentration (Di Risio and Yan, 2007). A screening of the viscosity dependence on CMC concentration and shear stress was performed in order to find an adequate CMC concentration, which would afford a viscosity value compatible with the gravure process (ideally 200 cP or higher). The curves for inks with 5, 6 or 7 mg/mL of CMC are shown in Fig. 2. It is clearly seen that the fluids are non-Newtonian, with viscosity depending on shear. Interestingly, when the limiting viscosity for infinite shear is calculated, it shows a dependence with CMC concentration that is roughly linear, as displayed in the inset of Fig. 2. As the level of stress experienced by the ink when spread by the doctor blade on the gravure cylinder is extremely high (shear rate in our printings at 1 m/s is estimated to be ~10^7 s^{-1}), we suppose it is a good approximation to consider the limiting viscosity as a guide to estipulate CMC concentration, and the linear relationship observed is very convenient for that. Pure CMC solutions were also tested and showed the exact same profile for the viscosity versus shear stress curves, and the measured viscosity values were very close to the ones obtained for the inks with all the components and the respective concentration of CMC (shown in Fig. 2), confirming that CMC is the determinant material for that property.

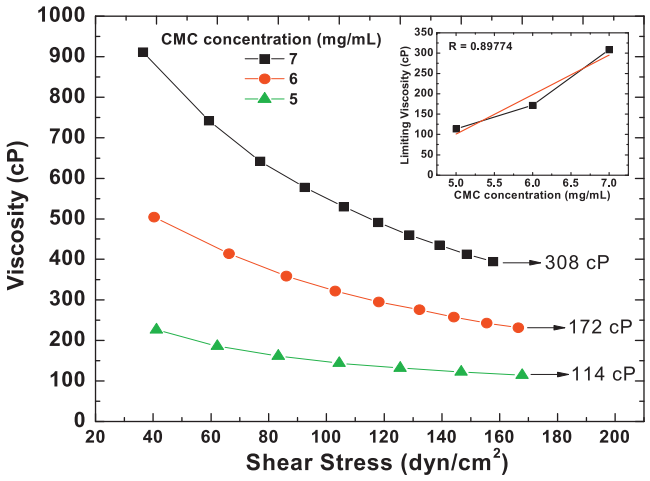

Fig. 2. Viscosity versus shear stress curves for inks with three different concentrations of carboxymethyl-cellulose (CMC) (all the other components used in the same amount). Inset: limiting viscosity calculated for an infinite shear stress versus CMC concentration.

The final ink formulation containing 1% w/v of trehalose, 0.05% v/v of triton X-100, 6 mg/mL of CMC and 68.5 of Tyr (hereafter named TyrInk) was tested in gravure printing, with the initial goal of addressing the effects from the printing process over enzyme activity (not concerning with good film formation). From the enzyme activity results for the ink before and after gravure printing and for control experiments, shown in Fig. 3, we can drawn two very important conclusions: (i) the use of the additives, which are needed to afford adequate viscosity and surface tension for printing, cause some damage to Tyr, decreasing its activity to 85.1% of its native activity in phosphate buffer pH 7.4 (taken as 100%); (ii) Despite the small initial activity loss caused by additives, we can clearly see that they are extremely helpful when TyrInk is printed. While Tyr completely loses its activity when a buffer solution is gravure printed (pink curve – kinetic compared to the negative control), it keeps an activity of 1372 U when printed in TyrInk, which is 15.5% of the native activity (or 18.2% of the initial 7521 U of the ink before printing). The residual activity of 15.5% after gravure printing is low at first glance, however, this is more than what was obtained for Tyr in Langmuir–Blodgett films successfully used as biosensors (Pavinatto et al., 2011).

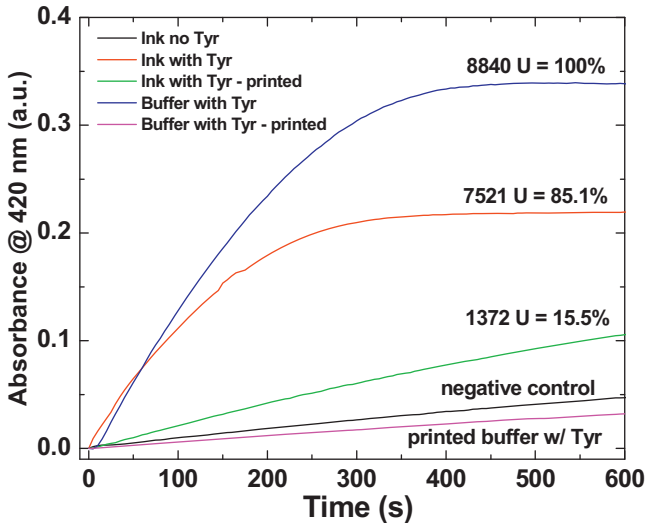

Fig. 3. Adsorption kinetics of purpurogallin generation catalyzed by the enzyme Tyr in different solutions, indicated in the graph. The control experiment (black curve) reflects the auto-oxidation of Pyr, without enzymatic catalyses (For interpretation of the references to color in this figure, the reader is referred to the web version of this article.).

3.3. *Gravure printing of Tyrosinase-containing ink*

After having its formulation established, TyrInk was tested in gravure printing on the plastics in which IDEs were previously printed, namely PET and PQA1. Two adjustable parameters in the GT1-5 print tester were optimized in order to transfer homogeneous films: printing speed (S) and the force (F) with which the gravure cylinder compress the substrate. After testing several combinations of these two parameters for printing on PET, it was seen that best results were obtained using $F=500$ N and $S=1$ m/s. However, even under these conditions, it was impossible to obtain a perfect coverage of the substrate with the ink. Films were macroscopically homogeneous, but when imaged under the microscope (Fig. 4A) a pattern of parallel stripes was seen, which is a reflex of improper ink spreading or dewetting after ink dispensing. The latter stressed the need for surface treatment, which was initially done with ozone irradiation for 10 min, but more effectively using oxygen plasma also for 10 min. While in the first case dewetting was still a problem, when the surface was made more hydrophilic by plasma treatment the ink could homogeneously spread forming the stable gravure printed film of TyrInk shown in Fig. 4B. In a macro-scale, this film is perfectly patterned with very well defined edges, as seen in Fig. 4C.

In the initial optimization for printing on PQA1, it was seen that the same combination of S and F have generated the best result, which shows that such parameters are strongly related to ink properties and does not strongly depend on ink–substrate interactions. Again, plasma treatment was vital for obtaining proper and stable spreading of the ink on the substrate, resulting in a homogeneous film as seen in Fig. 4D. Profilometry and AFM measurements were conducted for the films, but film thickness could not be obtained with precision because the plasticity of the substrate caused it to bend and deform during imaging.

Once conditions for printing on clean substrates were optimized, we proceeded to printing TyrInk on plastics having inkjetted electrodes printed on their surface. A typical result for Au IDEs on PQA1 is shown in Fig. 4E, and a similar behavior was observed for Ag on PET. Gravure printed films were again not homogeneous, showing stripes of material deposited alternately with regions of clean surfaces, for which dewetting or poor wetting has happened. In this case, the stripes were wider than the ones observed for substrates with no electrode printed on them (see Fig. 4A), showing that improper spreading is not too drastic. Moreover, as the printing support in this case (PQA1 with Au IDEs) was also treated with oxygen plasma for 10 min, as was bare PQA1, and since Au has a much higher free energy than the regions of exposed plastic, hindered flow of the ink is highly unexpected. From this, we can conclude that imperfections on film homogeneity were likely caused by the rough profile of the surface, constituted of 200–275 nm tall fingers (Fig. S1), which has probably triggered erratic ink flow during printing. Interestingly, such film imperfections allied to Au flatness and rigidity were convenient since they enabled good profilometry

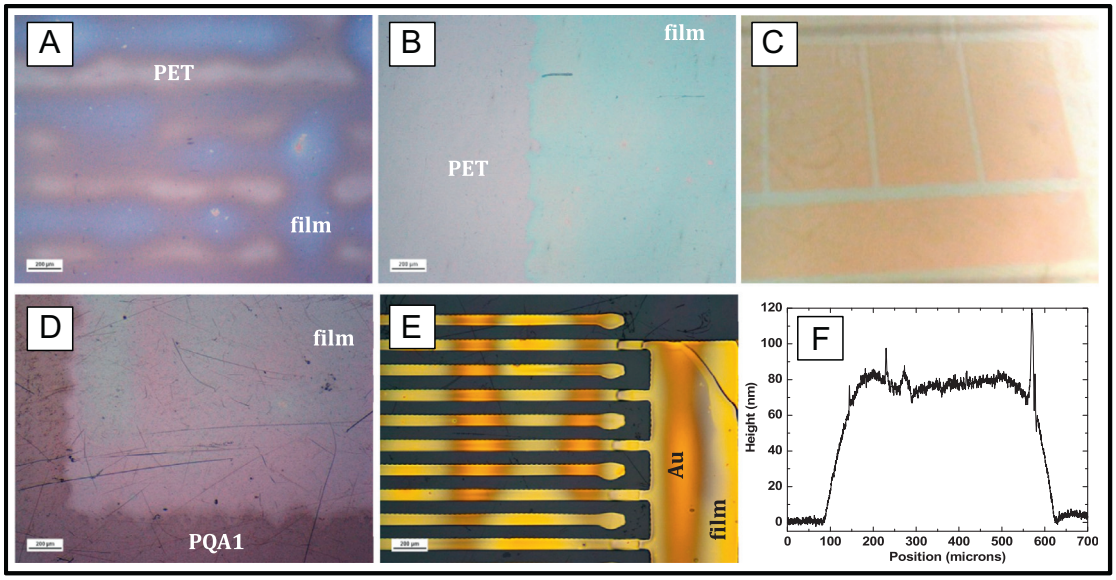

Fig. 4. Optical microscopy images of a typical gravure printed film of TyrInk on PET: (A) without and (B) with treatment with plasma; (C) digital photo of rectangular patterns of TyrInk film deposited over large areas of a PET sheet; (D) optical microscopy image of a TyrInk film gravure printed on a plasma treated PQA1 substrate; (E) optical microscopy image of a typical TyrInk film gravure printed on a plasma treated IDE electrode, previously inkjet-printed on PQA1; (F) line profile of the TyrInk gravure film on top of an ink-jetted Au finger.

measurements. The gravure printed TyrInk film in this case has thickness of 80 nm, as shown in Fig. 4F. This ultra-thin film is adequate for biosensing measurements since analyte can diffuse through the film, assessing more easily the active sites from the enzyme. As the erratic behavior discussed above is hard to avoid, since changes in electrodes geometry and shape are not desired, gravure printed films with the morphology shown in Fig. 4E were used in detection measurements.

3.4. Detection measurements

Initial tests using inkjet-printed Au and Ag IDEs electrodes coated with gravure printed films of TyrInk in biosensing measurements have exposed two different experimental issues. Firstly, it was promptly observed that the gravure printed films, which were processed from an aqueous-based ink were not sufficiently well adhered. Although scattered marks could be visually seen on the surface of the plastics after approximately 10 min of immersion of the biosensors in the measurement media, indicating the permanence of a very thin film of the active layer, most of the material was washed away and no patterned or homogeneous film remained on the surface. Such problem was solved by the use of a water-insoluble coating, which was applied to the surface of the printed active layer in order to avoid its dissolution. The material chosen for the coating was cellulose acetate (CA), a polysaccharide derivative already used for that goal (Setti et al., 2005; Yun et al., 2011), and encapsulation was done by a fast dip-coating deposition. CA concentration for the dip-coating solution was 10 times lower than what is usually employed in literature (Setti et al., 2005), and a film with an average thickness of 69 nm was deposited. The second problem observed was the lack of stability of Ag IDE electrodes that have deteriorated when immersed in buffer under the applied electric field used in impedance measurements. Surface darkening and partial dissolution were observed even when the electrodes were coated with a gravure film of TyrInk and the CA coating. Thus, only Au IDEs were employed here in detection measurements, and Ag IDEs will be explored in the future in sensors for gases.

Electrical impedance was measured for the biosensor in the range of frequencies between 5 Hz and 10 MHz in the absence and presence of the model antioxidant Pyr in different concentrations. A typical result, from where the detections curves were extracted is shown in Fig. S2. For some specific frequencies as 5 Hz and 1 kHz, impedance magnitude increases linearly with Pyr concentrations between 200 μm and 1.2 mM, as illustrated in Fig. 5A. This calibration curve shows that the printed biosensor is efficient at distinguishing antioxidant solutions with different concentrations in that range and can potentially be used to quantitative determine Pyr concentrations in solution. The detection mechanism in the impedance measurement is based on changes in dielectric constants and associated capacitances from different electrode–film–solution interfaces regions, which are caused by analyte diffusion and flow of electrons and small ions coming from the enzymatic reaction (Taylor and Macdonald, 1987; Zucolotto et al., 2006). Specifically at 5 Hz, where measurements were very reproducible, electrical double layer changes are assessed (Taylor and Macdonald, 1987). The leveling off of the impedance that happens for analyte concentrations above 1.2 mM is very likely due to the saturation of the film with adsorbed analyte.

Fig. 5B shows a reproduction of the linear part of the curve in 5 A (red curve) and the detection curve obtained for a second biosensor unit (green curve) prepared in another batch using the exact same conditions for the previous sensor (inkjet for electrodes and gravure for active layer). As it can be seen, the slope of the curves is approximately the same, corresponding to a sensitivity of 5.68 Ω/μm, which demonstrates good reproducibility in biosensor

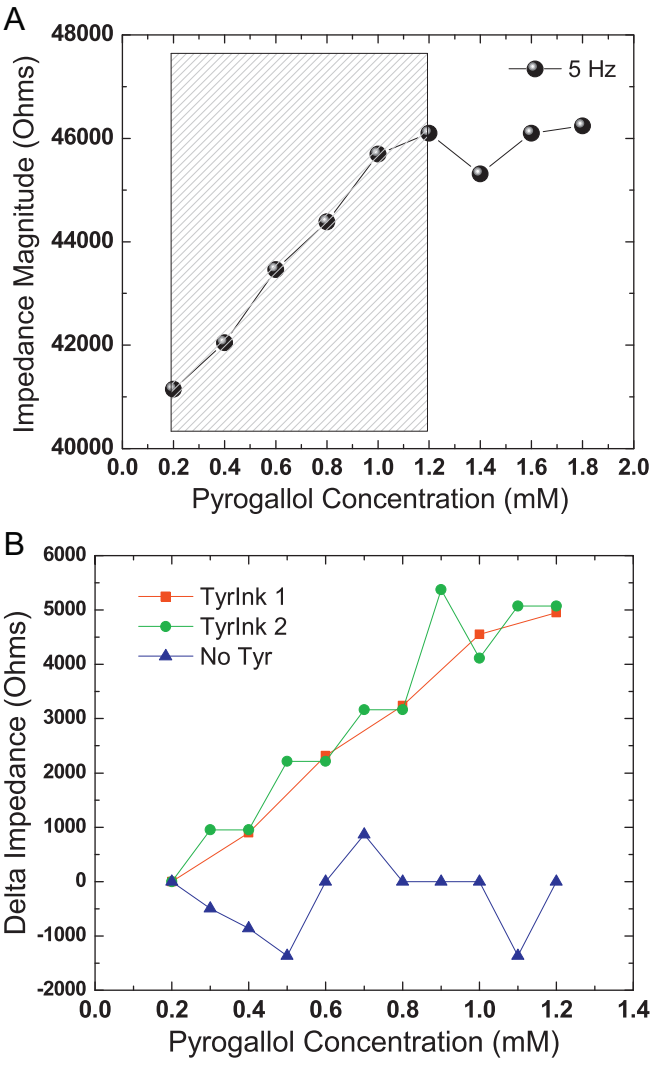

Fig. 5. A) Impedance magnitude at 5 Hz versus Pyr concentration, extracted from the curves in Fig. S2; (B) delta impedance (change in impedance relative to the absolute magnitude at 0.2 mM) versus Pyr concentration in buffer. The red curve shows only the linear part from the graph in (A), green curve is the data from an identical sensor fabricated in a different batch, and blue curve is the result from a sensor made using the same protocol, but with the enzyme Tyr being removed from the ink. (For interpretation of the references to color in this figure legend, the reader is referred to the web version of this article.)

fabrication using printing. However, from these pair of curves is also possible to see that sensor resolution is limited to 200 μM, since when additions of 100 μM are made (green curve) the sensor shows a ladder-like response and only impedances points measured after 200 μM coincide.

Two other control measurements were conducted. A bare Au IDE electrode was used in detection measurements for the same range of Pyr concentrations, but impedance magnitude in this case was very high (in the order of 10^7 Ω – the top limit for the equipment used) and no variations could be detected (result not shown). The second control measurement was conducted with a sensor unit made of a gravure-printed film of an ink with the same composition as TyrInk, but without the enzyme Tyr, which was deposited on top of an Au IDE. Impedance signal for this film (blue curve in Fig. 5B) shows a random fluctuation when antioxidant concentration is linearly increased. The latter unequivocally demonstrates the specificity inferred by Tyr when present in the active layer, and confirms the preserved activity of the enzyme

when deposited in the gravure film, already showed by optical measurements (Fig. 3).

4. Conclusions

An all-printed and flexible biosensor for antioxidants was successfully fabricated in this work. Interdigitated electrodes made of Au were directly deposited by inkjet in a one-step process using a commercial nanoparticle-based ink, which had its sintering conditions adapted to plastic-compatible temperatures. Traces with resolution of 45 μm and conductivity as high as 12% of bulk Au were printed and showed great stability to flexions and to the use in biosensing via impedance measurements. A tailor-made ink was prepared having 1% w/v of trehalose, 0.05% v/v of triton X-100, 68.5 μg/mL of Tyr and 6 mg/mL of CMC. This ink was efficiently gravure printed on plasma treated plastics, giving rise to homogenous patterned films. Additives are needed not only to provide a good printing, but also to improve enzyme stability and propitiate resistance to harsh gravure conditions, which resulted in 15.5% of preserved activity after printing. The printed biosensor has a sensitivity of 5.68 Ω/μm and limit of detection of 200 μM, which is well below the concentration of antioxidants in wines and olive oil (Carlsen et al., 2010). Due to the fast and large-area printing characteristics of gravure, and its compatibility with roll-to-roll (R2R) processes, it is believed that the biosensor fabricated here have great potential for the deployment of a technological product for the analysis of dietary products.

Acknowledgements

The authors would like to acknowledge Fundação de Amparo do Estado de São Paulo (Fapesp), which funded this research under project # 2011/05742-0. Also, we are grateful to Prof. Dr. Vivek Subramanian by the use of his printing-related facilities, Dr. Marcelo Assunção Pereira e Silva for complementary AFM measurements, and Prof. Dr. Antonio Riul Jr. for helpful discussions regarding the interpretation of impedance data. C.W.A. Paschoal acknowledges CNPq and CAPES Brazilian funding agencies, and R. Ramesh for all support at University of California.

Appendix A. Supplementary materials

Supplementary data associated with this article can be found in the online version at http://dx.doi.org/10.1016/j.bios.2014.09.039.

References

Abe, K., Suzuki, K., Citterio, D., 2008. Anal. Chem. 80, 6928–6934. http://dx.doi.org/10.1021/ac800604v.
Allen, M., Leppäniemi, J., Vilkman, M., Alastalo, A., Mattila, T., 2010. Nanotechnology 21, 475204. http://dx.doi.org/10.1088/0957-4484/21/47/475204.
Altenberend, U., Molina-Lopez, F., Oprea, A., Briand, D., Bârsan, N., De Rooij, N.F., Weimar, U., 2013. Sens. Actuators B Chem. 187, 280–287. http://dx.doi.org/10.1016/j.snb.2012.11.025.
Apetrei, C., Alessio, P., Constantino, C.J.L., de Saja, J. a, Rodriguez-Mendez, M.L., Pavinatto, F.J., Ramos Fernandes, E.G., Zucolotto, V., Oliveira, O.N., 2011. Biosens. Bioelectron. 26, 2513–2519. http://dx.doi.org/10.1016/j.bios.2010.10.047.
Arias, A.C., MacKenzie, J.D., McCulloch, I., Rivnay, J., Salleo, A., 2010. Chem. Rev. 110, 3–24. http://dx.doi.org/10.1021/cr900150b.
Arrabito, G., Galati, C., Castellano, S., Pignataro, B., 2013. Lab Chip 13, 68–72. http://dx.doi.org/10.1039/c2lc40948h.
Barroso, M.F., de-los-Santos-Álvarez, N., Delerue-Matos, C., Oliveira, M.B.P.P., 2011. Biosens. Bioelectron. 30, 1–12. http://dx.doi.org/10.1016/j.bios.2011.08.036.
Berggren, C., Bjarnason, B., Johansson, G., 2001. Electroanalysis 13, 173–180. http://dx.doi.org/10.1002/1521-4109(200103)13:3 < 173::AID-ELAN173 > 3.0.CO;2-B.
Carlsen, M.H., Halvorsen, B.L., Holte, K., Bøhn, S.K., Dragland, S., Sampson, L., Willey, C., Senoo, H., Umezono, Y., Sanada, C., Barikmo, I., Berhe, N., Willett, W.C., Phillips, R., Jacobs, D.R., Blomhoff, R., 2010. Nutr. J. 9, 3. http://dx.doi.org/10.1186/1475-2891-9-3.
Cho, H., Parameswaran, M., (Ash), Yu, H.-Z., 2007. Sens. Actuators B Chem. 123, 749–756. http://dx.doi.org/10.1016/j.snb.2006.10.022.
Claramunt, S., Monereo, O., Boix, M., Leghrib, R., Prades, J.D., Cornet, a., Merino, P., Merino, C., Cirera, a., 2013. Sens. Actuators B Chem. 187, 401–406. http://dx.doi.org/10.1016/j.snb.2012.12.093.
Correia, V., Caparros, C., Casellas, C., Francesch, L., Rocha, J.G., Lanceros-Mendez, S., 2013. Smart Mater. Struct. 22, 105028. http://dx.doi.org/10.1088/0964-1726/22/10/105028.
Delaney, J.T., Smith, P.J., Schubert, U.S., 2009. Soft Matter 5, 4866. http://dx.doi.org/10.1039/b909878j.
Derby, B., 2008. J. Mater. Chem. 18, 5717. http://dx.doi.org/10.1039/b807560c.
Derby, B., 2012. Science 338 (80), 921–926. http://dx.doi.org/10.1126/science.1226340.
Di Risio, S., Yan, N., 2007. Macromol. Rapid Commun. 28, 1934–1940. http://dx.doi.org/10.1002/marc.200700226.
Fraga, C.G., Galleano, M., Verstraeten, S.V., Oteiza, P.I., 2010. Mol. Asp. Med. 31, 435–445. http://dx.doi.org/10.1016/j.mam.2010.09.006.
Gonzalez-Macia, L., Morrin, A., Smyth, M.R., Killard, A.J., 2010. Analyst 135, 845–867. http://dx.doi.org/10.1039/b916888e.
Ilkhanizadeh, S., Teixeira, A.I., Hermanson, O., 2007. Biomaterials 28, 3936–3943. http://dx.doi.org/10.1016/j.biomaterials.2007.05.018.
Jabrane, T., Dubé, M., Griffiths, M., Mangin, P.J., 2011. J-FOR J. Sci. Technol. For. Prod. Process. 1, 6–13.
Jabrane, T., Jeaidi, J., Mangin, P.J., 2008. Adv. Print. Media Technol. 35, 279–288.
Kang, B., Lee, W.H., Cho, K., 2013. ACS Appl. Mater. Interfaces 5, 2302–2315. http://dx.doi.org/10.1021/am302796z.
Kaushik, J.K., Bhat, R., 2003. J. Biol. Chem. 278, 26458–26465. http://dx.doi.org/10.1074/jbc.M300815200.
Kipphan, H. (Ed.), 2001. Handbook of Print Media: Technologies and Production Methods. Springer, Heildelberg.
Mello, L.D., Kubota, L.T., 2007. Talanta 72, 335–348. http://dx.doi.org/10.1016/j.talanta.2006.11.041.
Monereo, O., Claramunt, S., Marigorta, M.M., De, Boix, M., Leghrib, R., Prades, J.D., Cornet, a, Merino, P., Merino, C., Cirera, a, 2013. Talanta 107, 239–247. http://dx.doi.org/10.1016/j.talanta.2013.01.022.
Pavinatto, F.J., Khan, Y., Arias, A.C., 2014. manuscript in preparation.
Pavinatto, F.J., Fernandes, E.G.R., Alessio, P., Constantino, C.J.L., de Saja, J. a., Zucolotto, V., Apetrei, C., Oliveira Jr, O.N., Rodriguez-Mendez, M.L., 2011. J. Mater. Chem. 21, 4995. http://dx.doi.org/10.1039/c0jm03864d.
Prieto-Simón, B., Cortina, M., Campàs, M., Calas-Blanchard, C., 2008. Sens. Actuators B Chem. 129, 459–466. http://dx.doi.org/10.1016/j.snb.2007.08.004.
Reddy, A.S.G., Narakathu, B.B., Atashbar, M.Z., Rebros, M., Rebrosova, E., Joyce, M.K., 2011a. Procedia Eng. 25, 956–959. http://dx.doi.org/10.1016/j.proeng.2011.12.235.
Reddy, A.S.G., Narakathu, B.B., Atashbar, M.Z., Rebros, M., Rebrosova, E., Joyce, M.K., 2011b. Procedia Eng. 25, 120–123. http://dx.doi.org/10.1016/j.proeng.2011.12.030.
Sanjana, N.E., Fuller, S.B., 2004. J. Neurosci. Methods 136, 151–163. http://dx.doi.org/10.1016/j.jneumeth.2004.01.011.
Saum, A.G.E., Cumming, R.H., Rowell, F.J., 2000. Biosens. Bioelectron. 15, 305–313.
Saunders, R., Gough, J., Derby, B., 2010. In: Ringeisen, B.R., Spargo, B.J., Wu, P.K. (Eds.), Cell and Organ Printing. Springer, Netherlands, Dordrecht, pp. 35–50. http://dx.doi.org/10.1007/978-90-481-9145-1.
Sen, S., Chakraborty, R., 2011. In: Andreescu, S. (Ed.), Oxidative Stress: Diagnostics, Prevention, and Therapy. American Chemical Society, Washington, DC, pp. 1–37.
Setti, L., Fraleoni-Morgera, A., Ballarin, B., Filippini, A., Frascaro, D., Piana, C., 2005. Biosens. Bioelectron. 20, 2019–2026. http://dx.doi.org/10.1016/j.bios.2004.09.022.
Singh, K.V., Bhura, D.K., Nandamuri, G., Whited, A.M., Evans, D., King, J., Solanki, R., 2011. Langmuir 27, 13931–13939. http://dx.doi.org/10.1021/la202546a.
Søndergaard, R.R., Hösel, M., Krebs, F.C., 2013. J. Polym. Sci. Part B Polym. Phys. 51, 16–34. http://dx.doi.org/10.1002/polb.23192.
Suman, O'Reilly, E., Kelly, M., Morrin, A., Smyth, M.R., Killard, A.J., 2011. Anal. Chim. Acta 697, 98–102. http://dx.doi.org/10.1016/j.aca.2011.04.036.
Sumerel, J., Lewis, J., Doraiswamy, A., Deravi, L.F., Sewell, S.L., Gerdon, A.E., Wright, D.W., Narayan, R.J., 2006. Biotechnol. J. 1, 976–987. http://dx.doi.org/10.1002/biot.200600123.
Taylor, D.M., Macdonald, a G., 1987. J. Phys. D. Appl. Phys., 20; , pp. 1277–1283. http://dx.doi.org/10.1088/0022-3727/20/10/010.
Tsouti, V., Boutopoulos, C., Zergioti, I., Chatzandroulis, S., 2011. Biosens. Bioelectron. 27, 1–11. http://dx.doi.org/10.1016/j.bios.2011.05.047.
Van Gerwen, P., Laureyn, W., Laureys, W., Huyberechts, G., Op De Beeck, M., Baert, K., Suls, J., Sansen, W., Jacobs, P., Hermans, L., Mertens, R., 1998. Sens. Actuators B Chem. 49, 73–80. http://dx.doi.org/10.1016/S0925-4005(98)00128-2.
Varshney, M., Li, Y., 2009. Biosens. Bioelectron. 24, 2951–2960. http://dx.doi.org/10.1016/j.bios.2008.10.001.
Villar, G., Graham, A.D., Bayley, H., 2013. Science 340, 48–52. http://dx.doi.org/10.1126/science.1229495.
Yun, Y.H., Lee, B.K., Choi, J.S., Kim, S., Yoo, B., Kim, Y.S., Park, K., Cho, Y.W., 2011. Anal. Sci. 27, 375.
Zucolotto, V., Pinto, A.P., Tumolo, T., Moraes, M.L., Baptista, M.S., Riul, A., Araújo, A.P. U., Oliveira, O.N., 2006. Biosens. Bioelectron. 21, 1320–1326. http://dx.doi.org/10.1016/j.bios.2005.06.001.